Contribution from the Department of Chemistry,
Northwestern University, Evanston, Illinois 60208-3113

Relationships between Structure and Redox Properties of $Ru_4(CO)_{12}(\mu_4\text{-}\eta^2\text{-}C_2Ph_2)$ and $[Et_4N]_2[Ru_4(CO)_{11}(\mu_4\text{-}\eta^2\text{-}C_2Ph_2)]$

Jiandang Wang, Michal Sabat, Leslie J. Lyons,*,† and Duward F. Shriver*

Received May 7, 1990

The cyclic voltammograms of $Ru_4(CO)_{12}(C_2Ph_2)$ (**1**) contain three irreversible peaks. The initial two-electron reduction of **1** is followed by loss of a CO ligand, and the product was identified spectroscopically in a bulk electrochemical experiment. This product, $[Et_4N]_2[Ru_4(CO)_{11}(C_2Ph_2)]$ (**3**), was also prepared independently by chemical reduction of **1** with Na/Hg. On the basis of variable scan rate experiments and the digital simulation of these cyclic voltammograms, the overall electrochemistry can be described by a mechanism involving at least six species. Of the six species, two (compounds **1** and **3**) have been isolated and structurally characterized. The electrochemistry of **3** was elucidated by variable scan rate experiments and digital simulation. A single-crystal X-ray structure determination of **3** reveals a dinegative anion containing a butterfly Ru_4 core, a $\mu_4\text{-}\eta^2\text{-}C_2Ph_2$ and two bridging and nine terminal CO ligands. Crystal data: monoclinic, a = 12.135 (1) Å, b = 18.078 (2) Å, c = 20.583 (2) Å, β = 104.79 (1)°, $P2_1/n$, Z = 4, final $R(F)$ = 0.031, $R_w(F)$ = 0.036.

Introduction

Since the first synthesis and structure determination of $Co_4(CO)_{10}(\mu_4\text{-}\eta^2\text{-}C_2Et_2)$,[1] many butterfly acetylene clusters have been reported.[2-7] One example is the ruthenium diphenyl acetylene complex $Ru_4(CO)_{12}(C_2Ph_2)$ (**1**) prepared by direct thermal reaction of $Ru_3(CO)_{12}$ with the alkyne (eq 1).[2] The framework

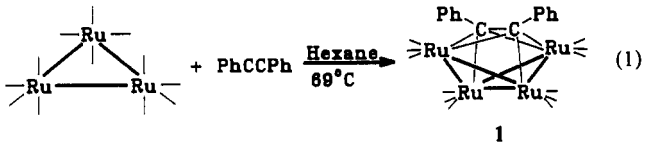

(1)

1

geometry of compound **1** can be described either as an M_4 butterfly with a $\mu_4\text{-}\eta^2$-alkyne ligand or as a *closo*-octahedron with four metal and two carbon atoms as the vertices. If viewed as a butterfly cluster, **1** has 60 cluster valence electrons (CVE), which are less than the 62 CVE required for a butterfly structure.[8] If viewed as a *closo*-octahedral cluster, it has 66 CVE, which are satisfactory for a four-metal two-carbon octahedron.[8] The electron counting rules facilitate structural correlations, but they do not necessarily provide insight into chemical properties, which depend on the finer details of the electronic structure. Redox chemistry is often a useful probe for the relative energies of frontier orbitals. For instance, we previously reported a facile one-electron reduction of the acyl carbide cluster derivatives $[Fe_4(CO)_{12}(CC(O)R)]^-$ (R = Me, CH_2Ph), which demonstrated that the electron adds to a low-lying metal-framework-based molecular orbital, and so, from this perspective, the 60-CVE butterfly description suits the parent cluster better than the *closo*-trigonal-bipyramidal description (eq 2).[9]

$$[Fe_4(CO)_{12}(CC(O)R)]^- \xrightarrow{e^-} [Fe_4(CO)_{12}(CC(O)R)]^{2-} \quad (2)$$

Although electrochemistry has revealed many important aspects of the electronic structures for several classes of metal clusters,[10] the redox properties of butterfly alkyne compounds such as **1** have received little attention. A detailed electrochemical study and the chemical reduction of compound **1** was prompted by our previous observations of the facile reduction of a cluster having an ambiguous electron count, eq. 2.

Experimental Section

Materials and Methods. All reactions and electrochemical experiments were carried out under anhydrous conditions in an air-free atmosphere of N_2 or CO.[11] Preparative thin-layer chromatography was performed in an N_2-purged elution chamber. Solvents were dried and distilled under N_2 prior to use: CH_2Cl_2 from P_2O_5, THF, and Et_2O, $(i\text{-}Pr)_2O$ from sodium benzophenone ketyl, and hexane and pentane from 4A molecular sieves.[12] The CH_3CN solvent used for electrochemical experiments was distilled from CaH_2, followed by vacuum distillation from P_2O_5 and storage over 4A molecular sieves.[9] $[Et_4N]BF_4$ was recrystallized from ethyl acetate/pentane. $C_6H_5C{\equiv}CC_6H_5$ (Aldrich), Hg (Goldsmith), Na (Aldrich), and silica gel (Aldrich, TLC high-purity grade) were used as received. The $[(n\text{-}Bu)_4N]BF_4$ (TBAFB) electrolyte was recrystallized twice from ethyl acetate/pentane and dried at 60 °C overnight before use.[9] The starting material $Ru_3(CO)_{12}$ was prepared by a literature method.[13]

Instrumentation and Measurements. Cyclic voltammetry (CV) and controlled-potential coulometry were carried out with a BAS-100A electrochemical analyzer. All CV data were corrected for *iR* by the positive feedback circuitry of the instrument based on the uncompensated solution resistance values determined in a 50-mV range where no electrolysis occurred. Cyclic voltammograms were obtained by using a cell with a three-electrode configuration consisting of a Pt-disk (diameter = 1.7 mm) working electrode and a Pt-coil counter electrode. A silver wire immersed in electrolyte solution was used as the quasi-reference electrode, which was contained in a glass tube, and it communicated with the analyte solution via a cracked glass tip. The reference potential was corrected to that of Ag/AgCl, either by using an internal Cp_2Fe standard or by comparing the CV's with those obtained with a commercial Ag/AgCl reference electrode (BAS). For the oxidation of Cp_2Fe in a 1 mM solution in TBAFB/CH_3CN, the potential value of +490 mV was ob-

† Current address: Department of Chemistry, Grinnell College, Grinnell, IA 50112.

(1) (a) Krüerke, U.; Hübel, W. *Chem. Ber.* **1961**, *94*, 2829-2856. (b) Dahl, L. F.; Smith, D. L. *J. Am. Chem. Soc.* **1962**, *84*, 2450-2452.
(2) (a) Johnson, B. F. G.; Lewis, J.; Schorpp, K. T. *J. Organomet. Chem.* **1975**, *91*, C13-C16. (b) Johnson, B. F. G.; Lewis, J.; Reichert, B. E.; Schorpp, K. T.; Sheldrick, G. M. *J. Chem. Soc., Dalton Trans.* **1977**, 1417-1419. (c) Jackson, P. F.; Johnson, B. F. G.; Lewis, J.; Raithby, P. R.; Will, G. J.; McPartlin, M.; Nelson, W. J. H. *J. Chem. Soc., Chem. Commun.* **1980**, 1190-1191.
(3) Granozzi, G.; Bertoncello, R.; Acampora, M.; Ajò, D.; Osella, D.; Aime, S. *J. Organomet. Chem.* **1983**, *244*, 383-391.
(4) (a) Gervasio, G.; Rossetti, R.; Stanghellini, P. L. *Organometallics* **1985**, *4*, 1612-1619. (b) Jackson, R.; Johnson, B. F. G.; Lewis, J.; Raithby, P. R.; Sankey, S. W. *J. Organomet. Chem.* **1980**, *193*, C1-C6.
(5) Roland, E.; Vahrenkamp, H. *Organometallics* **1983**, *2*, 183-184.
(6) (a) Aime, S.; Osella, D.; Milone, L.; Manotti Lanfredi, A. M.; Tiripicchio, A. *Inorg. Chim. Acta* **1983**, *71*, 141-147. (b) Jones, D. F.; Dixneuf, P. H.; Benoit, A.; Le Marouille, J.-Y. *J. Chem. Soc., Chem. Commun.* **1982**, 1217-1218. (c) Fox, J. R.; Gladfelter, W. L.; Geoffroy, G. L.; Tavanaiepour, I.; Abdel-Mequid, S.; Day, V. W. *Inorg. Chem.* **1981**, *20*, 3230-3237. (d) Osella, D.; Sappa, E.; Tiripicchio, A.; Camellini, M. T. *Inorg. Chim. Acta* **1980**, *42*, 183-190.
(7) (a) Sappa, E.; Tiripicchio, A.; Carty, A. J.; Toogood, G. E. *Prog. Inorg. Chem.* **1987**, *35*, 437-525. (b) Sappa, E.; Tiripicchio, A.; Braunstein, P. *Chem. Rev.* **1983**, *83*, 203-239.
(8) Lauher, J. W. *J. Am. Chem. Soc.* **1978**, *100*, 5305-5315.
(9) Wang, J.; Crespi, A. M.; Sabat, M.; Harris, S.; Woodcock, C.; Shriver, D. F. *Inorg. Chem.* **1989**, *28*, 697-703.
(10) Geiger, W. E.; Connelly, N. G. *Adv. Organomet. Chem.* **1985**, *24*, 87-130.
(11) Shriver, D. F.; Drezdzon, M. A. *The Manipulation of Air-Sensitive Compounds*, 2nd ed.; Wiley: New York, 1986.
(12) Gordon, A. J.; Ford, R. A. *The Chemist's Companion*; Wiley: New York, 1972.
(13) Bruce, M. I.; Matisons, J. G.; Wallis, R. C.; Patrick, J. M.; Skelton, B. W.; White, A. H. *J. Chem. Soc., Dalton Trans.* **1983**, 2365-2373.

0020-1669/91/1330-0382$02.50/0

Table I. Crystallographic Data for $[Et_4N]_2[Ru_4(CO)_{11}(C_2Ph_2)]$ (3)

formula: $C_{41}H_{50}O_{11}N_2Ru_4$	space group: $P2_1/n$ (No. 14)
fw: 1151.13	$T = -120$ °C
$a = 12.135$ (1) Å	$\lambda = 0.71069$ Å (Mo Kα)
$b = 18.078$ (2) Å	$\rho_{calcd} = 1.75$ g cm^{-3}
$c = 20.583$ (2) Å	$\mu = 13.89$ cm^{-1}
$\beta = 104.79$ (1)°	transm coeff = 0.94–1.12
$V = 4366$ (1) Å^3	$R(F) = 0.031$
$Z = 4$	$R_w(F) = 0.036$

served vs the Ag-wire quasi-reference electrode and repeated potential measurements against the Ag-wire electrode showed values within a ±40-mV range of that against the Ag/AgCl electrode. The solution used for CV was usually 100 mM in TBAFB ($[(n\text{-}Bu)_4N]BF_4$) and 1 to 2 mM in the electroactive species. Controlled-potential coulometry was performed using Pt gauze as the working and counter electrodes in a two-compartment electrolysis cell, with the compartments separated by a fine-porosity glass frit.

NMR spectra were recorded on a Varian XL400 (^{1}H, 400 MHz; ^{13}C, 101 MHz) spectrometer. Samples for ^{13}C NMR measurements were enriched to greater than 75% ^{13}CO by using published procedures.[9,14] Infrared spectra were recorded on a Mattson Alpha-Centauri FTIR spectrometer. Mass spectra were obtained for the cluster anion only by the liquid SIMS (secondary ion mass spectroscopy) technique in a *m*-nitrobenzyl alcohol matrix with CsI as the source for the Cs^+ primary ion beam for bombardment on a VG-70-series mass spectrometer. Elemental analyses were performed by Analytische Laboratorien Elbach, Engelskirchen, West Germany.

Digital Simulation of the Cyclic Voltammograms. Computations were performed on an IBM AT-compatible computer. The simulated CV's were generated by using the definite difference method of Feldberg.[15] A PASCAL program described each electrochemical step with the formal potential $E°$, standard heterogeneous electron-transfer rate parameter ψ, and electron-transfer coefficient α. For the irreversible electrochemical processes, ψ and α were determined from the experimental peak potential E_p, the half-peak potential $e_{p/2}$, and an arbitrary $E°$ by using the relationship[16]

$$\ln \psi = 0.780 + \ln (\alpha/\pi)^{1/2} + (\alpha nF/RT)(E_p - E°)$$

Since we saw no evidence for successive one-electron processes, the two-electron-transfer reactions were simulated as one-electron-transfer reactions and the current in the simulated CV was scaled to the experimental current in order to take account of the coulometric observation of $n = 2$.

Synthesis of $Ru_4(CO)_{12}(C_2Ph_2)$ (1). We followed a modification of the reported synthesis of $Ru_4(CO)_{12}(C_2Ph_2)$.[2] A solution of 565 mg (0.88 mmol) of $Ru_3(CO)_{12}$ and 200 mg (1.12 mmol) of $C_6H_5C_2C_6H_5$ in 50 mL of hexane was refluxed for 3 days. The solution was filtered hot, and the solvent was removed from the filtrate under vacuum. The solid was redissolved in 10 mL of CH_2Cl_2 and distributed among 10 thin-layer chromatographic plates (20 × 20 cm). After elution from a 1:9 mixed eluent of CH_2Cl_2 and hexanes (alternatively, a 3:17 mixture of CH_2Cl_2 and *n*-hexane), the brown band having the third largest R_f value was collected, which afforded 65 mg (0.07 mmol, 8%) of $Ru_4(CO)_{12}(C_2Ph_2)$. IR (ν_{CO}): in CH_2Cl_2, 2093.0 (w), 2067.0 (s), 2039.0 (s), 2015.4 (m), 1965.7 (w) cm^{-1}; in hexane, 2092.5 (m), 2081.4 (w), 2066.5 (vs), 2042.0 (vs, sh), 2039.5 (vs), 2018.8 (s), 2009.1 (m), 1989.8 (w), 1971.5 (m) cm^{-1}. These match the literature values.[2]

Synthesis of $[Et_4N]_2[Ru_4(CO)_{11}(C_2Ph_2)]$ (3). Sodium amalgam (~4%) was added slowly into a stirred solution of 18.5 mg of $Ru_4(CO)_{12}(C_2Ph_2)$ (0.020 mmol) in 10 mL of THF. The color of the solution changed from dark brown to bright red in ca. 5 min. IR spectra of the resulting solution revealed complete conversion of the starting compound to a dinegative anion.[14,17] The same product was obtained when the reaction was carried out under CO. This red solution was added to 10 mg (0.046 mmol) of $[Et_4N]BF_4$ solid, and the $NaBF_4$ precipitate was removed by filtration. The filtrate was concentrated to ca. 1 mL and layered with 20 mL of $(i\text{-}Pr)_2O$ in a diffusion tube, and 20 mg (0.017 mmol, 85%) of red crystals were obtained. IR (ν_{CO}) (THF): 2007.7 (m), 1963.8 (m), 1943.5 (s), 1904.5 (w), 1875.6 (w), 1756.9 (w, br) cm^{-1}.

Table II. Change of Peak Current Values (μA) with Continuous Scan Cycling in CV's of Compound **1** at 2 V s^{-1}

	i_p[a]		
cycle no.	peak a	peak b	peak c
1	20.1	10.6	0
2	13.8	12.0	~0.1
3	11.6	12.7	0.4
4	10.6	13.1	0.7
5	9.9	13.3	0.8
6	9.6	13.3	0.9

[a] Peak current values (in a 0.10 M TBAFB/CH_3CN solution) for the cathodic peaks a and c and for the anodic peak b.

Table III. Change of Peak Potential Values (mV) with Scan Rate (mV s^{-1}) in CV's of **1**

	E_p[a]		
scan speed	peak a	peak b	peak c
20	−668	+170	
100	−708	+190	
200	−720	+200	−828
500	−750	+214	−854
1003	−774	+226	−868
2007	−804	+238	−894
5120	−848	+270	−952

[a] Peak potential values vs Ag/AgCl (in 0.10 M TBAFB/CH_3CN) for the cathodic peaks a and c and for the anodic peak b.

Anal. Calcd for $C_{41}H_{50}O_{11}N_2Ru_4$: C, 42.78; H, 4.38; N, 2.43; Ru, 35.12. Found: C, 42.78; H, 4.03; N, 2.29; Ru, 34.60.

X-ray Data Collection and Structure Determination of $[Et_4N]_2[Ru_4(CO)_{11}(C_2Ph_2)]$ (3). All measurements were carried out on an Enraf-Nonius CAD4 diffractometer using Mo Kα radiation. Lattice parameters were determined by the least-squares refinement of the setting angles of 25 high-angle reflections. Intensities of the four standard reflections were measured every 3 h of X-ray exposure and showed no significant changes. Empirical absorption corrections were done by using the DIFABS program[18] with the transmission factors in the range 0.54–1.12. A summary of crystal data is presented in Table I.

All calculations were performed on a Micro Vax 3600 computer using the TEXSAN 4.0 crystallographic software package.[19] The structure was solved by direct methods (SHELXS 86).[20] Full-matrix least-squares refinement with anisotropic thermal parameters for all non-hydrogen atoms of the complex anion yielded the final R of 0.031 (goodness of fit = 0.94). All hydrogen atoms were found from the difference Fourier maps and included as fixed contributions to the structure factors. The largest residual peak in the final difference map was 0.52 e/Å^3 high. Atomic scattering factors were those tabulated by Cromer and Waber[21] with anomalous dispersion corrections taken from the literature.[22]

Oxidation of $[Et_4N]_2[Ru_4(CO)_{11}(C_2Ph_2)]$ (3). A small amount of $[Et_4N]_2[Ru_4(CO)_{11}(C_2Ph_2)]$ was dissolved in THF and 2 equiv of $[Cp_2Fe]PF_6$ added under CO. The characteristic color of $Ru_4(CO)_{12}(C_2Ph_2)$ (**1**) was observed, and IR spectra indicated quantitative conversion to compound **1** within 5 min.

Several attempts were made to perform the above oxidation reaction under CO-free conditions. In some reactions the solution was presaturated with N_2; in others N_2 was bubbled through the solution during the reaction. Judging from IR spectra, the product was a mixture that varied in composition from one experiment to the next.

Results and Discussion

Electrochemistry of $Ru_4(CO)_{12}(C_2Ph_2)$ (1). The cyclic voltammograms of $Ru_4(CO)_{12}(C_2Ph_2)$ at 1000 mV/s (**1**) show two irreversible cathodic peaks and one irreversible anodic peak (Figure 1). At scanning rates lower than 100 mV s^{-1}, only one reduction peak, peak a, was observed at −0.71 V vs Ag/AgCl. The first significant oxidation peak, peak b, is encountered at +0.19 V. At higher scanning rates, the first scan cycle still consists of only one

(14) Wang, J.; Sabat, M.; Horwitz, C. P.; Shriver, D. F. *Inorg. Chem.* **1988**, *27*, 552–557.
(15) Feldberg, S. W. In *Electroanalytical Chemistry*; Bard, A. J., Ed.; Marcel Dekker: New York, 1969; Vol. 3, pp 199–296.
(16) Bard, A. J.; Faulkner, J. R. *Electrochemical Methods: Fundamentals and Applications*; Wiley: New York, 1980; p 223.
(17) (a) Shriver, D. F.; Cooper, C. B., III. *Adv. Infrared Raman Spectrosc.* **1980**, *6*, 127–157. (b) Chini, P. *Inorg. Chim. Acta, Rev.* **1968**, *2*, 31–51.
(18) Walker, N.; Stuart, D. *Acta Crystallogr.* **1983**, *A39*, 158–166.
(19) Swepston, P. N. *TEXSAN 4.0, the TEXRAY Structure Analysis Program Package*; Molecular Structure Corp.: College Station, TX, 1987.
(20) Sheldrick, G. M. *SHELXS 86. A Program for Crystal Structure Determination*; University of Göttingen: Göttingen, FRG, 1986.
(21) *International Tables for X-ray Crystallography*; Kynoch: Birmingham, England, 1974; Vol. 4, pp 99–101.
(22) Reference 21, pp 149–150.

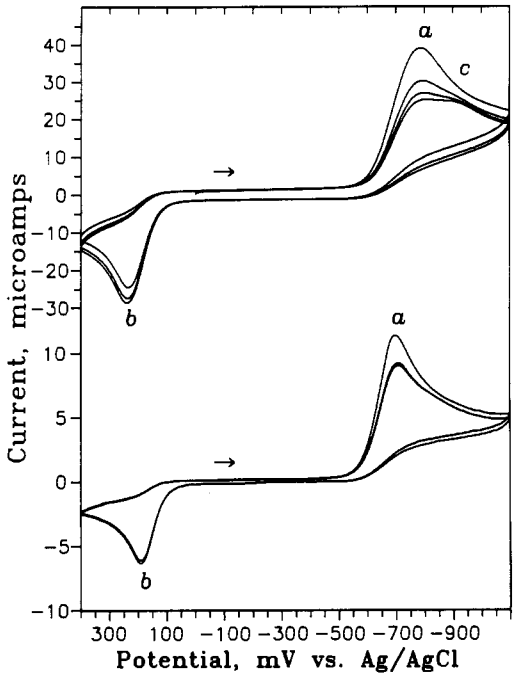

Figure 1. Cyclic voltammograms of $Ru_4(CO)_{12}(C_2Ph_2)$ (**1**), 2 mM solution in 0.10 M TBAFB/CH_3CN (Pt working electrode, Ag/AgCl reference), at scan rates of (top) 1000 mV s^{-1} and (bottom) 100 mV s^{-1}.

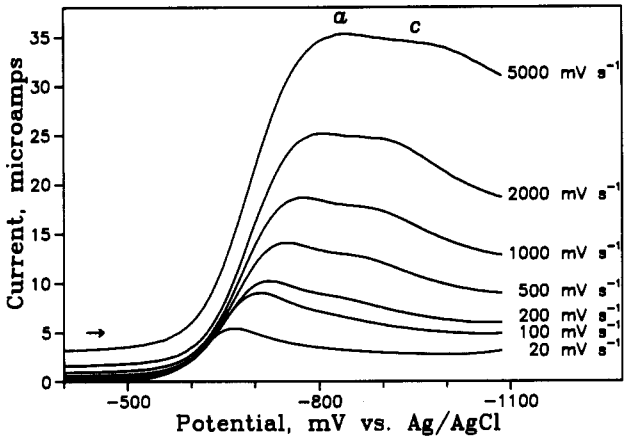

Figure 2. Portions of cyclic voltammograms of $Ru_4(CO)_{12}(C_2Ph_2)$ (**1**), 2 mM solution in 0.10 M TBAFB/CH_3CN (Pt working electrode, Ag/AgCl reference), at different scan rates.

reduction peak (a) and one oxidation peak (b), but another reduction peak, c, starts to grow in at −0.83 V in subsequent cycles. The peak current for peak a decreases and that for peak c increases with continuous cycling until a steady state is reached, whereas the peak current for peak b remains relatively constant (Table II). The sum of the peak currents for peaks a and c roughly equals the current for peak b. The steady-state peak current values for peak c relative to peak a increase as the scan rate is increased (Figure 2). Peak potential values for all three peaks change with scan rate (Table III). These changes in potential values are due to slow electron-transfer kinetics and not due to uncompensated solution resistance (iR_u), since measurements of the ferrocene peak separation under similar conditions were virtually independent of the scan rate. Peak b is observed only when the cathodic potential region of peak a has been scanned in the first half of the cycle. Similarly, the reduction peak c must be preceded by peak b. In other words, peak b is not observed if only the anodic potential region is scanned; this indicates that the species giving rise to peak b is derived from the species produced upon reduction a, and peak c represents a species produced subsequent to oxidation b. None of these features have associated return waves, suggesting that one or more facile chemical conversions follow each electron-transfer reaction. These observations are consistent with a

Scheme I

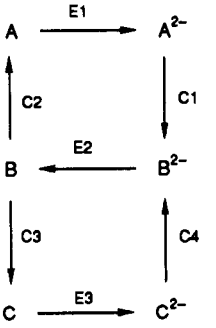

Table IV. Formal Rate Constants from Digital Simulation of CV's of **1**

reacn[a]	rate const,[b] cm s^{-1}	reacn[a]	rate const, s^{-1}
E1	0.018	C1	390
E2	0.122	C2	140
E3	0.014	C3	620
		C4	390

[a] Reaction steps as designated in Scheme I: E refers to electron transfer and C chemical conversion reactions. [b] For E1, E2, and E3, $k_s = \psi(\pi(38.92)D_0v))^{1/2}$, and for C1–C4, $k_{rxn} = \psi(38.92v)$, where v is the scan rate in V s^{-1} and D_0 is the diffusion coefficient. Used for the present calculations is the approximated value of $D_0 = 1 \times 10^{-5}$ cm^2 s^{-1}, which is typical of organometallic cluster species in nonaqueous solutions.[9,24]

series of electrochemical redox processes coupled with chemical conversion processes[23] described in Scheme I, where A is **1** and B^{2-} is the cluster anion of compound **3**. Constant potential electrolysis on the negative side of peak a (−1.0 V) consumed 2.1 F mol^{-1}, indicating that the reduction E1 produces A^{2-}. The similarity for currents for peaks b and c to that for peak a suggests that E2 and E3 in Scheme I might also be two-electron processes.

In this scheme, the neutral compound **1**, represented as A, is initially reduced by two electrons at −0.71 V (E1, peak a) to A^{2-}, which quickly converts to B^{2-} (chemical conversion C1). Oxidation of B^{2-} at +0.19 V (E2, peak b) produces B, which converts to A (C2) or to C (C3). The two chemical processes C2 and C3 can be either parallel (A ← B → C) or sequential (B → C → A). The reduction of C at −0.83 V (E3, peak c) is observed only when the potential is scanned at a fast rate, indicating that either species C is less stable than A or reaction C3 is faster than C2. Finally, upon reduction of C to C^{2-}, the latter quickly converts to B^{2-} (C4). The mechanism in Scheme I thus incorporates the following observations: (1) No return voltammetric waves are observed; (2) peak a precedes peak b, and peak b precedes peak c; (3) the sum of currents for peaks a and c approximately equals the current for peak b; and (4) on continuous cycling, the peak current decreases for peak a, increases for peak c, and does not change much for peak b.

Since none of the redox peaks in Figure 1 is reversible, kinetics data could not be obtained from simple electrochemical kinetic expressions. A dynamic model was therefore used to simulate the experiments digitally. As shown in Scheme I, the proposed three two-electron-transfer steps and the four chemical-conversion steps are coupled, which makes detailed simulation difficult. Two approximations were employed: (1) the electrochemical two-electron processes are treated as a one-electron transfer since the detailed microkinetics information on the individual one-electron steps is neither available nor of concern, and (2) a pseudo-first-order rate law is used for the chemical-conversion processes. The simulation program calculates the concentration of each of the six species according to Scheme I and then computes the faradic current as a function of potential as the reactions progress.[24]

(23) Reference 16, pp 213–248.
(24) Lyons, L. J. Ph.D. Thesis, University of Wisconsin—Madison, WI, Aug 1987.

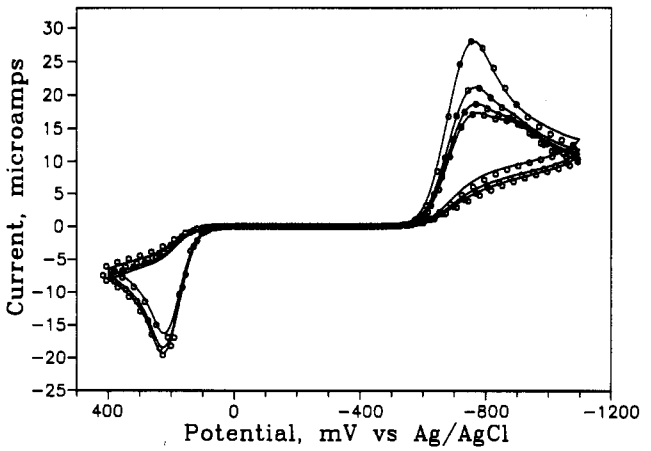

Figure 3. Simulated (open circles) and experimental (solid line) cyclic voltammograms of $Ru_4(CO)_{12}(C_2Ph_2)$ (**1**) at 1000 mV s^{-1}. Parameters used for the simulation: for E1, $\alpha = 0.41$, $\psi = 0.50$, $E° = 770$ mV; for E2, $\alpha = 0.50$, $\psi = 3.50$, $E° = -197$ mV; for E3, $\alpha = 0.55$, $\psi = 0.40$, $E° = 910$ mV; and, for the chemical steps, $\psi = 10.0$ (C1), 3.60 (C2), 16.0 (C3), and 10.0 (C4).

Figure 3 shows the fit between a simulated and an experimental CV at a 1000 mV s^{-1} scan rate. Good agreement between the experimental and simulated data was achieved in the scan rate range of 1000–5000 mV s^{-1}. We could not simulate the CV's for scan rates below 1000 mV s^{-1} (due to limitations of the computer) and did not acquire data for scan rates higher than 5000 mV s^{-1}. The reaction rate constants providing an acceptable fit are listed in Table IV. These are within the normal range of rate constants for the electron-transfer and the chemical steps.[25,26] The plausibility of the mechanism in Scheme I is thus supported by the successful description of the experimental CV's by the simulation. It should be borne in mind that since ψ and $E°$ are coupled mathematically the parameter set is not unique. Scheme I suggests that B^{2-} is the only stable species among the reduced products, and this prompted chemical reduction experiments in order to prepare bulk quantities of B^{2-}.

Synthesis of $[R_4N]_2[Ru_4(CO)_{11}(C_2Ph_2)]$ (3). The reduction of **1** can be carried out chemically by addition of sodium amalgam (eq 3). The sodium salt **2**, which gives the same IR spectra as

$$\underset{\mathbf{1}}{Ru_4(CO)_{12}(C_2Ph_2)} \xrightarrow[THF]{Na/Hg} \underset{\mathbf{2}}{Na_2[Ru_4(CO)_{11}(C_2Ph_2)]} + CO \quad (3)$$

the electrochemically observed species B^{2-} (Scheme I), was converted into the $[Et_4N]^+$ salt by metathesis (eq 4). The loss of

$$\underset{\mathbf{2}}{Na_2[Ru_4(CO)_{11}(C_2Ph_2)]} + 2\,[Et_4N]BF_4 \xrightarrow[THF]{} \underset{\mathbf{3}}{[Et_4N]_2[Ru_4(CO)_{11}(C_2Ph_2)]} + 2\,NaBF_4 \quad (4)$$

1 mol of CO in reaction 5 was confirmed by the mass spectrum ($M^+ = 892$ amu for the anion by the liquid SIMS technique in *m*-nitrobenzyl alcohol, with the appropriate CO dissociation and isotope peak patterns observed) and by the crystal structure determination of the final product **3**. Compound **3**, the $[Et_4N]^+$ salt, was isolated by filtration from the solid $NaBF_4$ and then crystallized by layering the concentrated filtrate with diisopropyl ether. The resulting red crystalline compound is relatively air-stable in the solid state but decomposes in solution quickly if exposed to air. Other $[R_4N]^+$ salts of $[Ru_4(CO)_{11}(C_2Ph_2)]^{2-}$ can be prepared by metathesis of **2** with simple salts of $[Me_4N]^+$, $[(n\text{-}Bu)_4N]^+$,

Table V. Selected Bond Distances (Å) in the Anion of **3**, $[Ru_4(CO)_{11}(C_2Ph_2)]^{2-}$

Ru(1)–Ru(2)	2.7555 (8)	Ru(2)–C(13)	2.325 (6)
Ru(1)–Ru(3)	2.8217 (9)	Ru(2)–C(14)	2.257 (6)
Ru(1)–Ru(4)	2.7318 (8)	Ru(3)–C(14)	2.231 (6)
Ru(2)–Ru(3)	2.7518 (8)	Ru(4)–C(13)	2.263 (6)
Ru(3)–Ru(4)	2.7232 (9)	Ru(4)–C(14)	2.261 (6)
Ru(1)–C(1)	1.896 (7)	C(14)–C(15)	1.519 (9)
Ru(1)–C(2)	1.892 (8)	C(13)–C(21)	1.500 (9)
Ru(1)–C(3)	1.887 (8)	O(1)–C(1)	1.146 (8)
Ru(2)–C(4)	1.846 (8)	O(2)–C(2)	1.156 (8)
Ru(2)–C(5)	1.859 (7)	O(3)–C(3)	1.159 (8)
Ru(2)–C(6)	1.982 (7)	O(3)–C(3)	1.159 (8)
Ru(3)–C(6)	2.116 (7)	O(5)–C(5)	1.161 (8)
Ru(3)–C(7)	1.905 (8)	O(6)–C(6)	1.193 (8)
Ru(3)–C(8)	1.883 (7)	O(7)–C(7)	1.134 (8)
Ru(3)–C(9)	2.225 (7)	O(8)–C(8)	1.153 (8)
Ru(4)–C(9)	1.981 (7)	O(9)–C(9)	1.169 (8)
Ru(4)–C(10)	1.868 (7)	O(10)–C(10)	1.159 (8)
Ru(4)–C(11)	1.859 (7)	O(11)–C(11)	1.158 (8)
Ru(1)–C(13)	2.187 (6)	C(13)–C(14)	1.422 (9)

Table VI. Selected Bond Angles (deg) in the Anion of **3**, $[Ru_4(CO)_{11}(C_2Ph_2)]^{2-}$

Ru(2)–Ru(1)–Ru(3)	59.11 (2)	Ru(1)–C(13)–Ru(2)	75.2 (2)
Ru(2)–Ru(1)–Ru(4)	92.98 (2)	Ru(1)–C(13)–Ru(4)	75.7 (2)
Ru(3)–Ru(1)–Ru(4)	58.70 (2)	Ru(2)–C(13)–Ru(4)	120.3 (3)
Ru(1)–Ru(2)–Ru(3)	61.64 (2)	Ru(2)–C(14)–Ru(3)	75.6 (2)
Ru(1)–Ru(3)–Ru(2)	59.25 (2)	Ru(2)–C(14)–Ru(4)	123.5 (3)
Ru(1)–Ru(3)–Ru(4)	59.00 (2)	Ru(3)–C(14)–Ru(4)	74.6 (2)
Ru(2)–Ru(3)–Ru(4)	93.25 (3)	Ru(1)–C(13)–C(14)	107.5 (4)
Ru(1)–Ru(4)–Ru(3)	62.30 (2)	Ru(2)–C(13)–C(14)	69.3 (3)
Ru(2)–Ru(1)–C(13)	54.7 (2)	Ru(4)–C(13)–C(14)	71.6 (3)
Ru(3)–Ru(1)–C(13)	72.9 (2)	Ru(2)–C(14)–C(13)	74.6 (3)
Ru(4)–Ru(1)–C(13)	53.4 (2)	Ru(3)–C(14)–C(13)	109.4 (4)
Ru(1)–Ru(2)–C(13)	50.1 (1)	Ru(4)–C(14)–C(13)	71.7 (3)
Ru(1)–Ru(2)–C(14)	71.2 (2)	Ru(3)–Ru(2)–C(6)	49.9 (2)
Ru(3)–Ru(2)–C(13)	72.4 (2)	Ru(1)–Ru(3)–C(6)	94.6 (2)
Ru(3)–Ru(2)–C(14)	51.8 (2)	Ru(4)–Ru(3)–C(9)	45.8 (2)
Ru(1)–Ru(3)–C(14)	70.2 (2)	C(14)–C(13)–C(21)	126.5 (5)
Ru(2)–Ru(3)–C(14)	52.6 (1)	C(13)–C(14)–C(15)	128.7 (6)
Ru(4)–Ru(3)–C(14)	53.2 (2)	Ru(2)–C(6)–Ru(3)	84.3 (5)
Ru(1)–Ru(4)–C(13)	50.9 (2)	Ru(2)–C(6)–O(6)	139.0 (5)
Ru(1)–Ru(4)–C(14)	71.6 (2)	Ru(3)–C(6)–O(6)	136.7 (5)
Ru(3)–Ru(4)–C(13)	73.8 (2)	Ru(3)–C(9)–Ru(4)	80.5 (3)
Ru(3)–Ru(4)–C(14)	52.2 (2)	Ru(3)–C(9)–O(9)	154.4 (5)
C(13)–Ru(2)–C(14)	36.1 (2)	Ru(4)–C(9)–O(9)	145.2 (6)
C(13)–Ru(4)–C(14)	36.6 (2)		

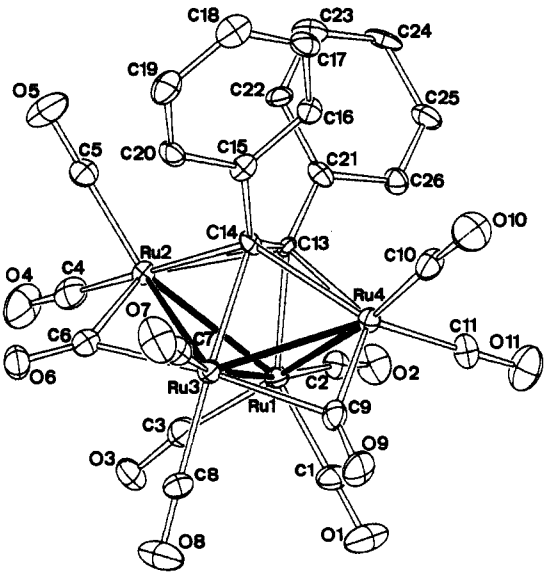

Figure 4. ORTEP diagram of the anion of **3**, $[Ru_4(CO)_{11}(C_2Ph_2)]^{2-}$. Thermal ellipsoids are drawn at the 50% probability level.

(25) Reference 16, p 227.
(26) (a) Atwood, J. D. *Inorganic and Organometallic Reaction Mechanisms*; Brooks/Cole: Monterey, CA, 1985. (b) Shen, J., Basolo, F., Northwestern University, private communication.
(27) Bradley, J. S. *Adv. Organomet. Chem.* **1985**, *22*, 1–58.
(28) Holt, E. M.; Whitmire, K. H.; Shriver, D. F. *J. Organomet. Chem.* **1981**, *213*, 127–137.
(29) Harris, S.; Blohm, M. L.; Gladfelter, W. L. *Inorg. Chem.* **1989**, *28*, 2290–2297.

Table VII. Comparison of Structural Data for Three Isoelectronic Clusters[a]

	$Ru_4(CO)_{12}(C_2Ph_2)$	$[Ru_4(CO)_{11}(C_2Ph_2)]^{2-}$	$Ru_2Co_2(CO)_{11}(C_2Ph_2)$
		Distances (Å)	
M_h–M_w[b]	2.71 (1)	2.7232 (9)	2.607 (1)
	2.74 (1)	2.7318 (8)	2.587 (1)
	2.71 (1)	2.7555 (8)	2.572 (1)
	2.74 (1)	2.7518 (8)	2.614 (1)
M_h–M_h	2.85 (1)	2.8217 (9)	2.757 (1)
M_h–C[c]	2.16 (1)	2.231 (6)	2.166 (3)
	2.16 (1)	2.187 (6)	2.278 (3)
M_w–C[c]	2.24 (1)	2.261 (6)	2.101 (3)
	2.24 (1)	2.263 (6)	2.048 (3)
	2.26 (1)	2.325 (6)	2.024 (3)
	2.25 (1)	2.257 (6)	2.102 (3)
C(13)–C(14)	1.46 (2)	1.422 (9)	1.432 (5)
		Angles (deg)	
C≡C–C	125.8 (9)	128.7 (6)	
	127.9 (10)	126.5 (5)	
M–M–M–M[d]	115.5	115.8	

[a] $Ru_4(CO)_{12}(C_2Ph_2)$ (**1**) ref 2c; $[Ru_4(CO)_{11}(C_2Ph_2)]^{2-}$, anion of **3**, present work; $[Ru_2Co_2(CO)_{11}(C_2Ph_2)]$, ref 5. [b] M_h and M_w refer to metal atoms at hinge and wingtip positions, respectively. [c] C represents the acetylenic carbon atoms: C(13) and C(14). [d] Dihedral angle between planes each defined by an M_w and the two M_h atoms.

and $[Me_3NCH_2Ph]^+$, among others. The bis(triphenylphosphine)nitrogen(1+) ($[PPN]^+$) salt can also be obtained by metathesis of **2** with [PPN]Cl.

Molecular Structure of $[Et_4N]_2[Ru_4(CO)_{11}(C_2Ph_2)]$ (3). One $[Ru_4(CO)_{11}(C_2Ph_2)]^{2-}$ and two $[Et_4N]^+$ units are located in the asymmetric unit of the crystal cell of **3**. The bond distances and angles for the anion $[Ru_4(CO)_{11}(C_2Ph_2)]^{2-}$ are presented in Tables V and VI, respectively. The ORTEP diagram for the anion (Figure 4) shows a butterfly arrangement of four ruthenium atoms. The alkyne ligand C_2Ph_2 is coordinated to all four metal atoms, as it is in the neutral parent cluster **1**. In Table VII, the bond distances and angles are compared between three isoelectronic clusters: the neutral cluster **1**, the anion of **3**, and $Ru_2Co_2(CO)_{11}(C_2Ph_2)$.[7] The M–M distances in **3** show no statistically significant changes as compared to **1**. All M–C distances to the acetylenic C atoms are similar to those in **1** except Ru(3)–C(14), which is elongated slightly (2.231 (6) as compared to 2.16 (1) Å in **1**). Attached to the four Ru atoms are eleven CO ligands, of which two, CO(6) and CO(8), bridge across the hinge and wingtip atoms of the butterfly. The other nine are terminal with normal bonding distances and angles (Ru–C + C–O = 3.01–3.05 Å and Ru–C–O = 171.7–178.5°, respectively).

The major structural changes upon conversion of **1** to **3** are the loss of a CO and the formation of two bridging CO groups, CO(6) and CO(9), which apparently fill the vacated coordination site. CO(6) is slightly more symmetrically bridging (Ru(2)–C(6)–O(6) = 139.0 (5)°, Ru(3)–C(6)–O(6) = 136.7 (5)°) than is CO(9) (Ru(4)–C(9)–O(9) = 145.2 (6)°, Ru(3)–C(9)–O(9) = 134.4 (5)°). Neither CO bridge, though, is totally symmetric: distances from C(6) or C(9) to the respective wingtip Ru atoms, 1.982 (7) or 1.981 (7) Å, are smaller than the distances to the hinge Ru(3) atom, 2.116 (7) or 2.225 (7) Å, respectively. The largest changes in geometry as a result of reduction occur around Ru(3). This metal atom connects to both bridging CO's, and its bond to the acetylenic carbon (Ru(3)–C(14)) is the only bond significantly lengthened. The two CO's bridge across two neighboring M–M bonds, leaving the cluster without a C_2 axis. On the other hand, the wingtip-to-hinge M–M bonds from one wingtip atom, Ru(2), are longer than those from the other. Ru(4), making the Ru(4) wing "smaller" than the Ru(2) wing of the butterfly structure.

Reoxidation of $[Et_4N]_2[Ru_4(CO)_{11}(C_2Ph_2)]$ (3). The chemical step that immediately follows reduction of **1** (reaction C1 in Scheme I, showing A^{2-} to B^{2-}) involves the loss of a CO ligand; therefore the conversion of B to A (C2) most likely involves CO association. In order to determine the CO involvement in these steps, cyclic voltammetry was performed on $[Et_4N]_2[Ru_4(CO)_{11}(C_2Ph_2)]$ (**3**) in the presence and absence of CO. The reduction region shows two peaks, a and c, under a CO atmosphere, but only one peak, c, under a nitrogen atmosphere (Figure 5). Since the peak currents for peaks a and c change with scan rate in the same fashion as those in the CV's of **1** (Figure 6), reaction C2 clearly is a CO addition reaction (eq 5). These results also indicate that no CO is involved in reaction C3.

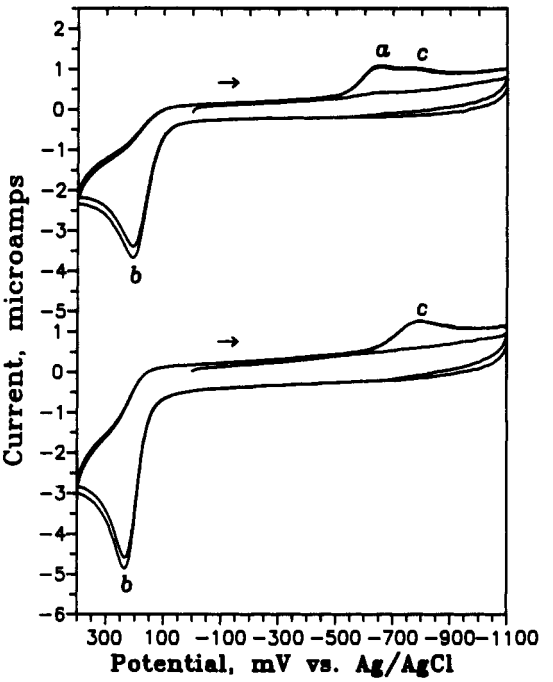

Figure 5. Cyclic voltammogram of $[Et_4N]_2[Ru_4(CO)_{11}(C_2Ph_2)]$ (**3**), 2 mM solution in 0.10 M TBAFB/CH_3CN (Pt working electrode, Ag/AgCl reference), at scan rate of 100 mV s^{-1}; (top) under CO; (bottom) under N_2.

$$\underset{B^{2-}}{[Ru_4(CO)_{11}(C_2Ph_2)]^{2-}} \xrightarrow[-2e^-]{} \underset{B}{[Ru_4(CO)_{11}(C_2Ph_2)]} \xrightarrow{CO} \underset{A\ (1)}{Ru_4(CO)_{12}(C_2Ph_2)} \quad (5)$$

Chemical reoxidation of B^{2-} by Cp_2Fe^+ under CO readily yields A, as shown in Scheme I. If CO is excluded, however, by an N_2 purge, IR spectra indicate that the oxidation yields a mixture of products that vary from one experiment to the next. Products having charges of 0, 1–, or 2– are inferred from the positions of the ν_{CO} bands.[17]

Conclusions

We have shown both electrochemically and chemically that $Ru_4(CO)_{12}(C_2Ph_2)$ (**1**) is easily reduced by a two-electron process

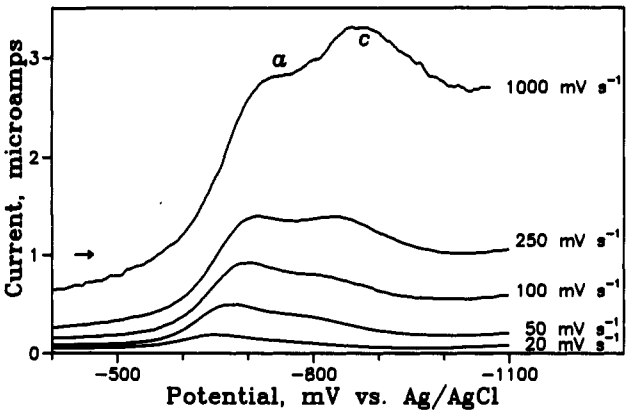

Figure 6. Negative-potential portions of the CV's of $[Et_4N]_2[Ru_4(CO)_{11}(C_2Ph_2)]$ (**3**) under CO (in 0.10 M TBAFB/CH_3CN, Pt working electrode, Ag/AgCl reference) at different scan speeds.

and that the reduction reaction is rapidly followed by the expulsion of a CO ligand. The dianion in the product $[Et_4N]_2[Ru_4(CO)_{11}(C_2Ph_2)]$ (**3**) is a *pseudooctahedral*-Ru_4C_2 cluster that contains two bridging CO groups. Structural comparisons between **3** and **1** revealed little change in the Ru_4C_2 core, indicating electronic stability of the cluster framework toward reduction. In light of the electrochemistry, the *closo*-octahedron description is, perhaps, most appropriate for these alkyne complexes. The isolation of compound **3** and successful digital simulation of the variable scan rate CV's of **1** agree with the mechanism represented in Scheme I.

Acknowledgment. We thank Eric J. Voss for the starting material $Ru_3(CO)_{12}$, Dr. Doris H. Hung for mass spectroscopy, Prof. David Phillips for helpful discussion, and Profs. A. M. Bond and J. W. Lauher for calling our attention to a possible connection between $[Fe_4(CO)_{12}(CC(O)R)]^-$ and the acetylene butterfly compounds. This research was supported by the NSF Synthetic Inorganic and Organometallic Chemistry Program through Grant CHE-8506011.

Supplementary Material Available: For **3**, tables of crystal structure data, positional parameters, thermal parameters, and all bond distances and angles and text describing the program for electrochemical simulation (24 pages); a complete listing of observed and calculated structure factors (27 pages). Ordering information is given on any current masthead page.

Contribution from the Department of Chemistry, University of Minnesota, Minneapolis, Minnesota 55455

Heterometallic Gold-Platinum Phosphine Complexes. 2. X-ray Crystal and Molecular Structures of $[(CO)(PPh_3)Pt(AuPPh_3)_5](Cl)$ and $[(PPh_3)Pt(AuPPh_3)_5(HgNO_3)_2](NO_3)$

Larry N. Ito, Anna Maria P. Felicissimo,† and Louis H. Pignolet*

Received July 13, 1990

In this paper we report the nucleophilic addition reaction of X^- (X = Br, I, CN) and the nucleophilic addition/substitution reaction of tertiary phosphites L = $P(OMe)_3$ or $P(OCH_2)_3CCH_3$ to the 16-electron cluster $[(PPh_3)Pt(AuPPh_3)_6]^{2+}$ (**7**), giving the new 18-electron complexes $[(X)(PPh_3)Pt(AuPPh_3)_6]^+$ (**9**) and $[(L)_2Pt(AuPPh_3)_6]^{2+}$ (**10**), respectively. An unusual oxidative-addition reaction of $Hg_2(NO_3)_2$ to **7** with elimination of $AuPPh_3^+$ giving the 18-electron product $[(PPh_3)Pt(AuPPh_3)_5(HgNO_3)_2]^+$ (**11**) has also been carried out. These reactions are shown in Scheme II. Some nucleophilic and electrophilic addition reactions that illustrate the above reactivity priniciple and that give six new $PtAu_x$ clusters with x = 3 and 4 have also been carried out as shown in Scheme I. These complexes have been characterized by IR, FABMS, and ^{31}P and ^{13}C NMR spectroscopy. X-ray crystal structure determinations have been carried out on the 18-electron clusters $[(CO)(PPh_3)Pt(AuPPh_3)_5]^+$ (**8**) and $[(PPh_3)Pt(AuPPh_3)_5(HgNO_3)_2]^+$ (**11**), and their metal core geometries, which are spheroidal fragments of centered icosahedrons, are in agreement with predictions based on electron counting. The crystal data for these complexes are as follows. **8**(Cl)·$(CH_3CH_2)_2O$: monoclinic, $C2/c$, a = 35.91 (1) Å, b = 29.637 (7) Å, c = 26.025 (7) Å, β = 132.62 (2)°, V = 20,383 Å^3, Z = 8; residuals R = 0.075 and R_w = 0.085 for 4815 observed reflections and 263 variables; Mo Kα radiation. **11**(NO_3)·$3CH_2Cl_2$: triclinic, $P\bar{1}$, a = 14.18 (1) Å, b = 17.92 (1) Å, c = 22.91 (2) Å, α = 89.68 (7)°, β = 84.80 (7)°, γ = 69.18 (7)°, V = 5415 Å^3, Z = 2; residuals R = 0.062 and R_w = 0.073 for 7822 observed reflections and 411 variables; Mo Kα radiation.

Introduction

A number of platinum-centered heterobimetallic cluster complexes of the general formulation $[(L)_yPt(AuPPh_3)_x]^{n+}$, where L = ligand (for example PPh_3, CO, RC≡C, H, NO_3) and/or metal (for example Ag or Hg) and x = 2, 6, 7, and 8, have recently been reported. Some of the well-characterized examples include $[(PPh_3)_2(NO_3)Pt(AuPPh_3)_2]^+$,[1] $[(C{\equiv}C{-}t\text{-}Bu)(PPh_3)Pt(AuPPh_3)_6]^+$,[2] $[(PPh_3)Pt(AuPPh_3)_6]^{2+}$,[3] $[(CO)(PPh_3)Pt(AuPPh_3)_6]^{2+}$,[3] $[(PPh_3)(H)Pt(AuPPh_3)_7]^{2+}$,[4,5] $[Pt(AuPPh_3)_8]^{2+}$,[6] $[(CO)Pt(AuPPh_3)_8]^{2+}$,[6] $[(AgNO_3)Pt(AuPPh_3)_8]^{2+}$,[7] $[(AgNO_3)(CO)Pt(AuPPh_3)_8]^{2+}$,[7] and $[(Hg)_2Pt(AuPPh_3)_8]^{4+}$.[8,9] These complexes form a series of $PtAu_x$ clusters that have shown a variety of novel structures and interesting reactivity.[1-10] In this paper we report the synthesis and characterization of six new $PtAu_x$ clusters with x = 3 and 4 (complexes **1-6** in Scheme I) and thus add the important missing members of the x = 2-8 series. Such a complete series of cluster complexes should prove important in studies of metal-particle physics, chemical bonding, reactivity,

† Institute of Chemistry, University of São Paulo, São Paulo, Brazil.

(1) Boyle, P. D.; Johnson, B. J.; Alexander, B. D.; Casalnuovo, J. A.; Gannon, P. R.; Johnson, S. M.; Larka, E. A.; Mueting, A. M.; Pignolet, L. H. *Inorg. Chem.* **1987**, *26*, 1346.
(2) Smith, E. W.; Welch, A. J.; Treurnicht, I.; Puddephatt, R. J. *Inorg. Chem.* **1986**, *25*, 4616.
(3) Ito, L. N.; Sweet, J. D.; Mueting, A. M.; Pignolet, L. H.; Schoondergang, M. F. J.; Steggerda, J. J. *Inorg. Chem.* **1989**, *28*, 3696.
(4) Kanters, R. P. F.; Bour, J. J.; Schlebos, P. P. J.; Bosman, W. P.; Behm, H.; Steggerda, J. J.; Ito, L. N.; Pignolet, L. H. *Inorg. Chem.* **1989**, *28*, 2591.
(5) Bour, J. J.; Kanters, R. P. F.; Schlebos, P. P. J.; Steggerda, J. J. *Recl. Trav. Chim. Pays-Bas* **1988**, *107*, 211.
(6) Kanters, R. P. F.; Schlebos, P. P. J.; Bour, J. J.; Bosman, W. P.; Behm, H. J.; Steggerda, J. J. *Inorg. Chem.* **1988**, *27*, 4034. Bour, J. J.; Kanters, R. P. F.; Schlebos, P. P. J.; Bosman, W. P.; Behm, H.; Beurskens, P. T.; Steggerda, J. J. *Recl.: J. R. Neth. Chem. Soc.* **1987**, *106*, 157. Bour, J. J.; Kanters, R. P. F.; Schlebos, P. P. J.; Steggerda, J. J. *Recl.: J. R. Neth. Chem. Soc.* **1988**, *107*, 211.
(7) Kanters, R. P. F.; Schlebos, P. P. J.; Bour, J. J.; Bosman, W. P.; Smits, J. M. M.; Beurskens, P. T.; Steggerda, J. J. *Inorg. Chem.* **1990**, *29*, 324.

0020-1669/91/1330-0387$02.50/0